Shear-Induced Aggregation of Colloidal Particles: A Comparison between Two Different Approaches to the Modelling of Colloidal Interactions

Graziano Frungieri[1] and Marco Vanni*,[1]

Department of Applied Science and Technology, Politecnico di Torino, Corso Duca degli Abruzzi 24, 10129 Torino, Italy

The process of shear-induced aggregation of fully destabilized colloidal suspensions has been investigated by adopting a mixed deterministic-stochastic modelling method. This method is based on a combination of a Monte Carlo algorithm, used to solve in a stochastic way the population balance equation for a purely aggregating suspension, and a Discrete Element Method, employed to simulate aggregation events in a fully predictive manner. The DEM was built in the framework of the well-established Stokesian dynamics technique to get an accurate prediction of the hydrodynamic forces acting on the primary particles. Two different approaches were instead used to describe colloidal interactions: the first assumes primary particles to interact only by means of central forces; a second model assumes also tangential interactions to act on primary particles upon contact. To describe such interactions we adopted a spring-like force model recently proposed by Becker and Briesen. Simulations were performed to ascertain the effect of these two different modelling approaches on the process of aggregation, showing that substantial differences appear in the predicted cluster morphology.

Keywords: colloidal suspensions, shear aggregation, Monte Carlo

INTRODUCTION

Aggregation plays a key role in a wide variety of industrial and natural processes involving colloidal suspensions. In the treatment of waste water, for instance, the aggregation of suspended particles is induced in order to generate large clusters that can be more effectively removed from the dispersing medium. In such processes aggregation is performed in mechanically stirred devices to favour the mixing of the flocculating agents and to speed up the growth of the aggregates. The velocity gradients of the flow field are capable of promoting encounters between the suspended particles, which may end up in their aggregation if the attractive interactions overcome the viscous resistance. At large Péclet numbers this mechanism, typically referred to as *orthokinetic aggregation*, prevails over the *perikinetic aggregation* driven by the Brownian motion of the particles. A number of works addressed this phenomenon both experimentally and numerically in simple laminar flows or turbulent conditions.[1–7]

The evolution of a population of colloidal particles is often modelled by resorting to Population Balance Equations (PBE).[8,9] These equations, obtained by simply imposing the conservation of mass throughout the aggregation process, are usually written in terms of one or more internal properties of the dispersed particles (e.g. mass, length, composition) and give the change in time of the distribution of such properties over the whole population. This approach dates back to the work by Von Smoluchowski,[10] who first employed PBE to study aggregating systems where the only internal variable was the number of primary particles in the aggregate.

Unfortunately, because of the complex nature of PBE, the solution of these equations by analytical methods is possible in a limited number of situations only; as a consequence a number of approaches have been used to calculate their solution numerically including sectional methods,[11–14] methods of moments,[15–17] and Monte Carlo techniques.[18–22] Monte Carlo (MC) schemes are a class of stochastic methods that adopt a limited number of simulated particles to reproduce the behaviour of an entire population of real particles. Because of their discrete nature, MC schemes are well suited to simulate an intrinsically discrete process such as aggregation. Their wide use is also due to the ability to follow the history of each simulated particle and handle easily complex multivariate populations, i.e. populations characterized by several internal variables.

Even if PBE, solved in a deterministic or stochastic way, may suffice to study aggregating systems, there exist alternative methods better suited to address the characterization of cluster morphology. Among these, Discrete Element Methods (DEM) represent a valid option; DEM simulations assume the clusters to be composed by a number of distinct elements, each one undergoing forces arising from the interaction with nearby elements and with the dispersing medium.[23] Introducing models for such interactions, DEM simulations are capable of tracking the motion of each individual particle of a cluster, providing valuable insight into the aggregation dynamics.[24] Several works employed the so called free draining approximation to model hydrodynamic interactions in DEM simulations,[25–29] assuming each particle to be subject to the Stokes drag force as if no other particle were present. Such an approach inevitably overestimates the hydrodynamic force acting on particles, especially on those placed in the inner region of a cluster, where significant shielding effects take place. In some studies the problem was approached by reducing the drag force on the basis of the effective portion of the surface of the particle exposed to the flow, estimated by simple geometrical

*Author to whom correspondence may be addressed.
E-mail address: marco.vanni@polito.it
Can. J. Chem. Eng. 95:1768–1780, 2017
© 2017 Canadian Society for Chemical Engineering
DOI 10.1002/cjce.22843
Published online 17 April 2017 in Wiley Online Library (wileyonlinelibrary.com).

considerations.[30,31] A more rigorous method is Stokesian dynamics, which is based on a truncated multi-pole expansion of the actual flow field. Stokesian dynamics is capable of giving accurate prediction of the hydrodynamic force and torque acting on each primary particle and for this reason it was widely employed in DEM simulations.[32–42]

In most of the studies employing DEM simulations, the DLVO theory (Derjaguin-Landau-Verwey-Overbeek) is adopted to model colloidal interactions among primary particles; these forces act along the centre-to-centre vector of two interacting particles and give the interparticle bond only a resistance to traction and compression.[24] However, it was shown that bonds are also capable of withstanding, to a certain extent, tangential stresses and bending moments.[43,44] On the basis of this observation, Becker and Briesen[45] developed a spring-like force model that, by introducing restoring forces and torques, was proven to properly capture the stiffness of the aggregates and the resistance exhibited by them against flow-induced deformation.[25] A number of rather similar models were proposed recently in the literature: Kroupa et al.,[29] in their study of systems undergoing coagulation and breakup, adopted the method proposed by Marshall,[46] who extended the traditional spring-dashpot-slider used by Cundall and Strack for sliding resistance;[23] Inci et al.[47] modelled non-central interactions between adjacent particles via a 3-body angular potential, by modifying the ESPResSo Molecular Dynamics code used by Isella and Drossinos.[24]

The present work aims to study the aggregation of aqueous dilute suspensions of colloidal particles under the effect of a spatially uniform shear flow. Simulations were performed starting from a mono-disperse population of spherical polystyrene particles with 500 nm radius. Two different populations were used: one composed by primary particles interacting solely by central forces, i.e. forces acting along the centre-to-centre vector; and a second one composed by particles that also show tangential and torsional resistance upon contact, according to the model proposed by Becker and Briesen.[45] Stokesian dynamics was employed to model hydrodynamic interactions.

To circumvent the high computational cost required by DEM simulations of populations of many aggregates, we integrated our DEM model with a Monte Carlo algorithm. The basic idea behind such a combination is that, if the suspension is sufficiently dilute, the aggregation dynamics is governed by a sequence of binary aggregation events. Therefore we used a Monte Carlo algorithm to sample a statistically expected sequence of such events and a DEM simulation to accurately reproduce them. The combination of these two computational methods allowed us to obtain reliable information regarding the dynamics of the process and the morphology of the aggregates. It should be observed that the existing literature concerning the application of DEM to colloidal systems is focused on restructuring and breakup.[25,27,38] To our knowledge, the role of interparticle interactions on the dynamics of pure aggregation and the morphology of the clusters obtained by such a process have not been investigated in detail so far, and still need to be clarified.

NUMERICAL METHOD

The dynamics of an aggregating colloidal system can be assumed to be determined by a sequence of distinct and separated in time aggregation events. In suspensions characterized by a low solid fraction it is reasonable to neglect multi-body interactions and assume each aggregation as a binary event, i.e. an event involving two aggregates at once. In a suspension, all aggregation events are preceded by encounters between suspended aggregates; if the suspension is stirred, the velocity gradients of the flow field bring aggregates close to each other, to a distance for which the probability of aggregation becomes significant. If the convective transport operated by the flow field and the colloidal attractive interaction are able to overcome the viscous resistance, the two aggregates may collide, causing the formation of a new larger aggregate; an *aggregation* event would therefore occur. A *missed aggregation* may occur as well: aggregates may pass close to each other without forming a new bond and therefore without a new aggregation. The actual outcome of an encounter is the consequence of a series of factors acting in a coordinate way: attractive colloidal forces enhance the aggregation probability, whereas hydrodynamic interaction may act preventing collisions; both kinds of interactions are dependent upon the morphology and the orientation of the approaching aggregates. It is apparent that all these factors need to be properly addressed in order to ascertain in a predictive way the outcome of each encounter event.

In this work we adopted an event-driven, rejection-free Monte Carlo (MC) algorithm to study the dynamic evolution of colloidal suspensions; the MC is used to reproduce a particular realization of the process through the generation of random sequences obeying the statistical laws that also govern the studied aggregation process. As it will be shown later, by defining the encounter properly, the expected encounter frequency can be evaluated a priori. The outcome of the encounter event is instead determined by using a detailed Discrete Element Method simulation (DEM), counting for both colloidal and hydrodynamic interactions.

Since the system is uniform, in order to reduce the computational cost, only a small fraction ΔV of the suspension was actually simulated, as suggested by Liffman;[18] however, the size of the simulated subvolume was adjusted during the simulation. The reduction of the number of aggregates occurring throughout the simulation as a consequence of aggregation would undermine the statistical robustness of the results; therefore, to avoid such a problem, the volume ΔV was doubled and all the aggregates cloned whenever the number of aggregates dropped below a threshold value (set equal to $3N_0/4$, N_0 being the initial number of simulated aggregates).

Monte Carlo Algorithm

In his seminal work Von Smoluchowski obtained a simple expression to model the two body aggregation rate in a laminar shear flow.[10] His analysis was limited to the case of solid spherical particles moving along the straight streamlines of the undisturbed flow field and aggregating irreversibly upon contact. However, in a colloidal suspension of spherical primary particles, upon aggregation, clusters with irregular shapes are generated and moreover colloidal and fluid dynamic interactions between approaching aggregates may substantially change the aggregation kinetics. For these reasons we adopted the approach by Von Smoluchowski to solely model the expected pair encounter frequency, with the actual outcome of the event being determined a posteriori by a DEM simulation. Figure 1 illustrates the typical configuration of an encounter involving two aggregates i and j in a shear flow of rate $\dot{\gamma} = \frac{\mathrm{d}u_z^{\infty}}{\mathrm{d}y}$. The size of the aggregates is characterized through the outer radius, computed as $R = \max_k (|\mathbf{x}_k - \mathbf{x}_{cm}|) + a$, where $|\mathrm{x}_k - \mathrm{x}_{cm}|$ is the distance of the k-th primary particle, with radius a, from the centre of mass of the aggregate. An encounter occurs whenever aggregate j passes close to aggregate i after crossing the "encounter cross-section." Such a cross-section is a circle of

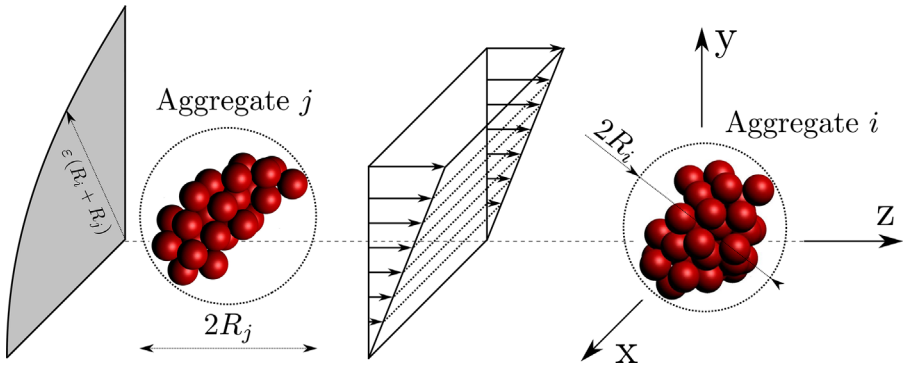

Figure 1. Representation of a shear-induced encounter between aggregate i and aggregate j in a reference system centred in the centre of mass of aggregate i. The grey region represents a quarter of the encounter cross-section. An encounter occurs whenever an aggregate j crosses the section.

radius $\varepsilon(R_i + R_j)$ centred on the z-axis, lying on a plane perpendicular to the z-axis and located far upstream from aggregate i, as shown in Figure 1. Hence, the frequency of an encounter is the same as the frequency at which j crosses the cross-section. For the evaluation of this frequency Von Smoluchowski's approach can be applied because, far from aggregate i, aggregate j moves along the streamlines of the undisturbed shear flow. Therefore, in a volume ΔV, the expected shear-induced encounter frequency between the pair of aggregates i,j reads as:

$$f_{ij} = \frac{4}{3}\dot{\gamma}\left[\varepsilon\left(R_i + R_j\right)\right]^3 c_i c_j \Delta V \tag{1}$$

where ε is a parameter used to set the amplitude of the collision cross-section. The value of ε was set equal to 0.5 for all collisions except those between primary particles, where we prescribed $\varepsilon = 1$. Preliminary tests ensured all the aggregation events were captured using such values. The terms c_i and c_j represent the number concentrations of aggregate i and j, both equal to $1/\Delta V$, because only one i-aggregate and one j-aggregate are present in the suspension. Finally, after defining $R_{ij} = R_i + R_j$, the expression for the encounter frequency becomes:

$$f_{ij} = \frac{4}{3}\dot{\gamma}\frac{\varepsilon^3 R_{ij}^3}{\Delta V} \tag{2}$$

In the presence of N_a suspended aggregates the total encounter frequency is given by:

$$f_{tot} = \sum_{i}^{N_a}\sum_{j=i+1}^{N_a} f_{ij} \tag{3}$$

We used this piece of information to estimate the time interval elapsing between two subsequent encounters. As reported by Shah et al. studying a rather similar birth-death process,[48] given an encounter event occurred at time t_0, the total frequency computed as in Equation (3) can be used to estimate the probability for a new event to take place at time $t = t_0 + \Delta t$ as:

$$Pr\left(\Delta t\right) = 1 - e^{-f_{tot}\Delta t} \tag{4}$$

Therefore Δt can be considered as an interval of quiescence (IQ) i.e. a waiting time during which no encounter occurs. Since the phenomena are stochastic, the IQ can be sampled resorting to its cumulative distribution function:[48] a random number is sampled from a uniform distribution between 0 and 1 and the IQ determined according to Equation (4).

The Monte Carlo method was used to select the aggregates involved as well. The probability for a generic encounter k between aggregates i and j to occur is:

$$Pr_k = f_{ij}/f_{tot} \tag{5}$$

After ordering properly the list of possible events, the event can be selected by picking a random number η from a uniform distribution between 0 and 1. The chosen event is that with the index q that satisfies the following relationship:

$$\sum_{k=1}^{q-1} Pr_k < \eta < \sum_{k=1}^{q} Pr_k \tag{6}$$

Once the involved aggregates are chosen, their initial spatial coordinates have to be determined in order to launch the DEM simulation of the encounter: at the beginning of each DEM simulation, the centre of mass of aggregate i is placed in the origin of the reference system; aggregate j is instead located far upstream from aggregate i and inside the encounter cross-section. Assuming the concentration of aggregates to be spatially uniform in the suspension, the position of the j aggregate can be determined on the basis of statistical considerations: far from aggregate i the translational velocity of aggregate j equals the undisturbed fluid velocity, $\dot{\gamma}y\mathbf{e}_z$, aligned to direction z, linearly increasing with y and independent of x. The probability for particle j to pass the encounter cross-section at a certain x,y coordinate has to reproduce such a distribution. If we examine the square with side εR_{ij} enclosing the encounter cross-section, as shown in graph (a) of Figure 2, the initial coordinates (x_j^0, y_j^0) for aggregate j can be determined by picking up a pair of random numbers from a uniform probability distribution for x (graph b) and a linear probability distribution for y (graph c), respectively. If the obtained coordinates lie outside the circular cross-section, they are discarded and the sampling is repeated until a pair of valid coordinates is obtained. The z_j^0-coordinate is set equal to $\pm 5R_{ij}$ (with the $\pm$ sign determined according to the sign of the y-coordinate): at this distance the hydrodynamic interactions acting between the two aggregates are negligible and we can assume that, in this initial configuration, the aggregates have the same velocity as the undisturbed fluid.

The next step of the method consists in the detailed simulation of the encounter by means of the Discrete Element Method. The DEM tracks the motion of each primary particle of the

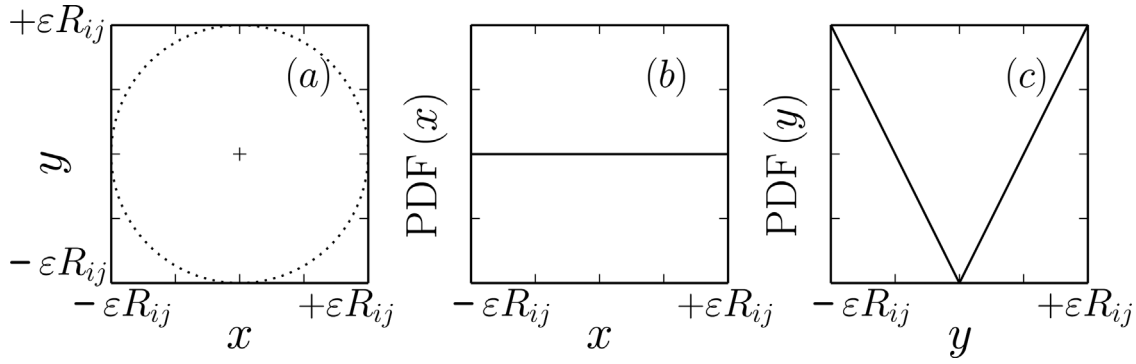

Figure 2. (a) Encounter cross-section on a *x*-*y* plane. Probability distribution for aggregate *j* to flow through the encounter cross-section at a given *x* (b) and *y* (c).

approaching aggregates and evaluates the effective outcome of the encounter and the geometry of the aggregates at the end of the process.

On the basis of the number of distinct aggregates identified at the end of the DEM simulation, the effect of the encounter event can be recognized; two qualitatively different outcomes are possible:

- *a missed collision*, that is, a close pass of the two aggregates without an actual collision and with no change of the number of primary particles in each aggregate;
- *an aggregation*, meaning that the two aggregates collide forming one stable, larger aggregate with the consequent net loss of one aggregate from the population.

A temporary aggregation, soon followed by a detachment, with or without an exchange of primary particles, is also possible in principle, but occurred very rarely. In any case, such a situation was easily handled by the DEM method. In any of the mentioned cases, even if no collision occurred, the fluid stresses exerted on the cluster structure can rearrange the positions of the primary particles, deforming the overall morphology of the aggregates. Although such a rearrangement occurs during the whole life of an aggregate, for the sake of simplicity, we took this effect into account only during encounters, assuming that the geometry of the aggregates remains frozen when not involved in an encounter.

Due to the changes in geometry, the birth of new aggregates, and the death of old ones originated by the aforementioned events, all the encounter frequencies of Equation (2) involving any of the aggregates returning from the DEM simulation need to be updated or calculated ex-novo after the encounter.

DEM Model

The Discrete Element Method tracks the trajectory of all the primary particles composing the aggregate by solving their individual equations of motion, taking into account the colloidal interactions and the hydrodynamic stresses exerted by the moving fluid.

Hydrodynamic interaction

Hydrodynamic interactions were evaluated by using Stokesian dynamics,[49] which is a well-established numerical method capable of accurately modelling the behaviour of a suspension in the Stokes flow regime. A detailed description of the technique can be found in Durlofsky et al.[50] For our purposes it suffices to say that Stokesian dynamics relates in a linear way the forces and torques acting on each of the N primary particles of the system with their relative velocity with respect to the surrounding fluid:

$$[\mathcal{R}] \cdot \begin{Bmatrix} \mathbf{u}_1 - \mathbf{u}_\infty(\mathbf{x}_1) \\ \vdots \\ \mathbf{u}_N - \mathbf{u}_\infty(\mathbf{x}_N) \\ \boldsymbol{\omega}_1 - \boldsymbol{\omega}_\infty \\ \vdots \\ \boldsymbol{\omega}_N - \boldsymbol{\omega}_\infty \end{Bmatrix} = - \begin{Bmatrix} \mathbf{F}_1^H \\ \vdots \\ \mathbf{F}_N^H \\ \mathbf{T}_{(1)}^H \\ \vdots \\ \mathbf{T}_N^H \end{Bmatrix} + [\mathcal{S}] \cdot \begin{Bmatrix} -\mathbf{E}_\infty \\ \vdots \\ -\mathbf{E}_\infty \\ -\mathbf{E}_\infty \\ \vdots \\ -\mathbf{E}_\infty \end{Bmatrix} \tag{7}$$

where indicating by α a generic primary particle, the vectors $\mathbf{u}_\alpha$ and $\boldsymbol{\omega}_\alpha$ are respectively the linear and angular velocity of the α-th primary particle, whereas $\mathbf{u}_\infty(\mathbf{x}_\alpha)$ is the velocity of the undisturbed velocity field evaluated at the centre of the α-th suspended monomer. Our simple shear flow gives the undisturbed linear velocity field $\mathbf{u}_\infty(\mathbf{x}) = \dot{\gamma} y \mathbf{e}_z$, with $\mathbf{e}_z$ being the unit vector aligned to the z direction, whereas the undisturbed fluid angular velocity $\boldsymbol{\omega}_\infty$ and the deformation rate tensor $\mathbf{E}_\infty$ do not depend on the position $\mathbf{x} = (x, y, z)$ and their only non-zero elements are $\omega_{\infty,x} = \dot{\gamma}/2$ and $E_{\infty,yz} = E_{\infty,zy} = \dot{\gamma}/2$. The terms $\mathbf{F}_\alpha^H$ and $\mathbf{T}_\alpha^H$ contain the components of the hydrodynamic force and torque acting on the α-th monomer. It can be shown that the components of matrices $[\mathcal{R}]$ and $[\mathcal{S}]$ depend only on fluid viscosity, size, and relative positions of the primary particles.[51] These resistance matrices are built from two contributions: a far field component obtained from a truncated multi-pole expansion of the flow field describes correctly the interactions between particles that are relatively far apart, and a near field correction based on lubrication theory is valid when particles are in close proximity. As usual in this type of simulations,[52–54] a *cut-off length scale* δ has been introduced to avoid the singularity of lubrication force occurring when particles get in contact: when the gap h between two approaching particles becomes smaller than δ, the applied pair lubrication correction is no longer updated, but kept evaluated at $h = \delta$. In the simulations we adopted $\delta = 0.1$ nm.

Colloidal interaction

Traditionally the colloidal interactions between primary particles are modelled according to the classical DLVO theory, by introducing forces acting exclusively along the centre-to-centre line. However, it has been recently demonstrated that between bonded particles there exists a tangential interaction capable of supporting tangential stress and bending moments.[43] To take into account such interactions we adopted a model recently proposed by Becker

and Briesen for DEM simulations,[45] which is able to give torsional, rolling, and sliding resistance to the bond between two particles by replacing the bond with a number of fictitious springs.

In order to assess the effect of tangential interactions we simulated the aggregation behaviour for two different populations of primary particles:

- Population A, composed by primary particles interacting only by means of central forces;
- Population B, composed by particles interacting by means of both central and tangential forces.

Central forces model Different expressions were used in this case for the interaction of a pair of particles before and after contact. When the particles are in proximity but not in contact, the usual expression for the Van der Waals attraction between spheres was employed:[55]

$$F^{vdw} = \frac{A_H \cdot a}{12 \cdot (h + z_0)^2} \cdot g\,(h) \tag{8}$$

where A_H is the composite Hamaker constant for the interaction of two solids immersed in a third medium, and z_0 is the minimum approach distance (assumed to be equal to 0.165 nm). The term $g(h)$ takes into account the retardation effect, which determines a steeper decrease of the total interaction at large separation. This effect was modelled according to:[56]

$$g\,(h) = \begin{cases} \frac{1+3.54p}{\left(1+1.77p^2\right)} & 0 < p < 0.5709 \\ \\ \frac{0.98}{p} - \frac{0.434}{p^2} + \frac{0.067429}{p^3} & 0.5709 < p < \infty \end{cases} \tag{9}$$

where $p = 2\pi(h + z_0)/\lambda$, with λ, assumed equal to 100 nm, being the characteristic wavelength of the dispersion interaction.

After the interparticle contact is established, the joint effect of adhesive forces and elastic response of the material is modelled according to the contact mechanics theory by Johnson, Kendall, and Roberts (JKR).[57] In the theory contacting particles are subject to elastic deformation. The intensity of the total interaction force, F^{coll}, is plotted in Figure 3 as a function of the surface-to-surface distance h normalized by the common primary particle radius a. Positive values of F^{coll} correspond to a repulsive force, and negative values to an attractive one. The gap distance is defined as $h = d_{\alpha\beta} - 2a$, where $d_{\alpha\beta}$ is the centre-centre distance

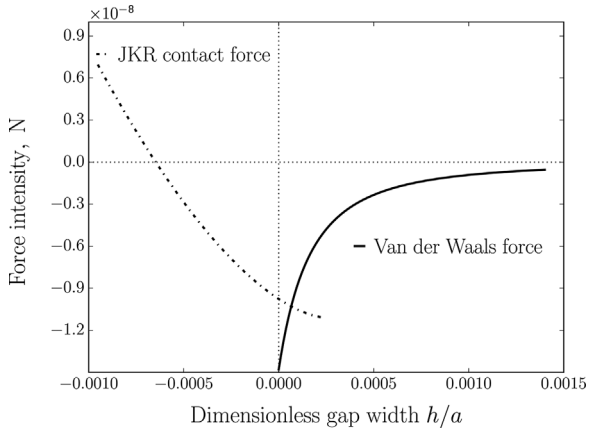

Figure 3. Model adopted for the central colloidal interaction between primary particles. Van der Waals: Equation (8); JKR: Equation (10).

between the two particles. Before contact h is the actual surface-to-surface distance between the spheres. After contact, however, h is determined by the deformation of the surfaces and can take on negative values.

For a pair of contacting particles the theory provides the following relationship between the force acting at the contact along the normal direction, F^{JKR}, and the surface-to-surface distance, h:

$$h = \frac{b_0^2}{a}\left(\frac{1+\sqrt{1+F^{JKR}/F^{adh}}}{2}\right)^{1/3} \cdot \left(\frac{1-3\sqrt{1+F^{JKR}/F^{adh}}}{3}\right) \tag{10}$$

where the zero-load contact radius is given by $b_0 = \left(9\pi\gamma_s a^2\left(1-\nu^2\right)/2E\right)^{1/3}$, with γ_s being the surface energy of the solid and where ν and E are respectively the Poisson ratio and the elastic modulus of the primary particles. The adhesive force of the contact i.e. the largest traction force that the contact can bear, is given by:

$$F^{adh} = \frac{3}{2}\pi\gamma_s a. \tag{11}$$

When this adhesive force is exceeded, the detachment takes place at a pull-off distance h equal to:

$$h_{po} = \left(\frac{3\pi^2\gamma_s^2 a\left(1-\nu^2\right)^2}{8E^2}\right)^{1/3} \tag{12}$$

As can be noticed in Figure 3 our model is composed by two distinct curves (Van der Waals and JKR interaction, that act before and after contact, respectively). It also includes hysteresis in order to properly model the complex contact-detachment dynamics occurring in the presence of large adhesion forces.

The primary particles of Population A interact exclusively by the central force model outlined up to here. As a consequence, two of these primary particles are able to withstand the tensile stresses that would pull them away, but no force hinders the other modes of relative displacements, such as mutual rolling or sliding.

Tangential forces model In addition to the central force, the particles of Population B also interact by means of tangential forces and bending moments; as shown by Pantina and Furst,[43] the large adhesion force between two bonded colloidal particles is able to also hinder the relative displacement along the contact surface. Several methods were proposed to model such interactions and to provide a level of resistance to sliding, rolling, and twisting. Inci[47] modelled non-central interactions between adjacent particles via a 3-body angular potential using an approach typical of Molecular Dynamics. Marshall[46] extended the traditional spring-dashpot-slider model of DEM by introducing three different models to hinder each of the possible relative motion modes along the contact plane. A more compact model was proposed by Becker and Briesen;[45] their model is able to couple the rolling and sliding resistance by introducing a simple rod-spring system (Figure 4), whose parameters are derived from the experimental observation by Pantina and Furst. We adopted this latter model to give twisting, rolling, and sliding resistance to the monomer-monomer bonds of Population B.

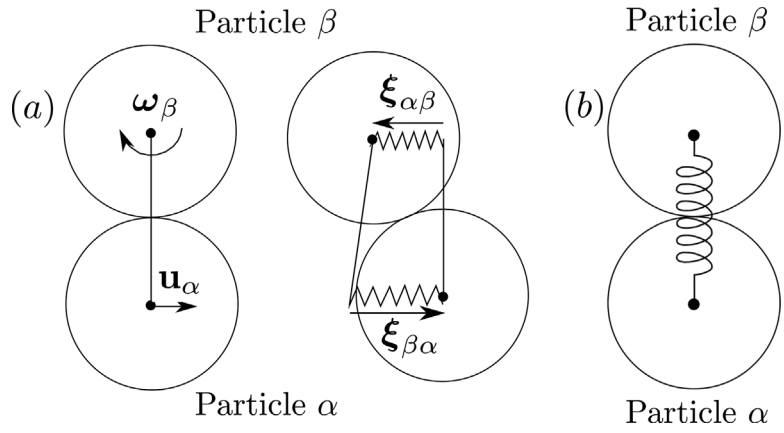

Figure 4. Model adopted for the tangential interaction between bonded primary particles. (a) Tangential springs; (b) torsional spring.

With regard to Figure 4, two springs are initialized when the particles come into mechanical contact. Denoted by $\xi_{\alpha,\beta}$ and $\xi_{\beta,\alpha}$ the elongations of the springs induced by the relative tangential velocity, the restoring forces can be computed as:

$$\mathbf{F}_\alpha = k_t\left(\boldsymbol{\xi}_{\alpha,\beta} - \boldsymbol{\xi}_{\beta,\alpha}\right) \qquad \mathbf{F}_\beta = k_t\left(\boldsymbol{\xi}_{\beta,\alpha} - \boldsymbol{\xi}_{\alpha,\beta}\right) \tag{13}$$

while the corresponding torques as:

$$\mathbf{T}_\alpha = 2ak_t\mathbf{x}_{\alpha,\beta} \times \boldsymbol{\xi}_{\alpha,\beta} \qquad \mathbf{T}_\beta = -2ak_t\mathbf{x}_{\alpha,\beta} \times \boldsymbol{\xi}_{\beta,\alpha} \tag{14}$$

where k_t is the stiffness of the springs and $\mathbf{x}_{\alpha,\beta}$ is the vector pointing from the centre of particle α to the centre of particle β. In a similar fashion, a torsional spring is also introduced when two particles get in contact. Denoting by $\phi_{\alpha,\beta}$ the twisting angle of the spring, the restoring torque is given by:

$$\mathbf{T}_\alpha = -\mathbf{T}_\beta = k_\phi\phi_{\alpha,\beta}\mathbf{x}_{\alpha,\beta} \tag{15}$$

The torsional stiffness k_ϕ and the tangential stiffness k_t, as well as the corresponding maximal spring elongations ϕ_{max} and ξ_{max}, were estimated as described in the work by Becker and Briesen.

Encounter dynamics

The motion of every primary particle of the simulated aggregates can be described by the equations of motion:

$$\begin{cases} m\frac{d\mathbf{u}_\alpha}{dt} = \mathbf{F}_\alpha^H + \mathbf{F}_\alpha^{coll} \\ I\frac{d\boldsymbol{\omega}_\alpha}{dt} = \mathbf{T}_\alpha^H + \mathbf{T}_\alpha^{coll} \end{cases} \tag{16}$$

where m and I are the mass and the moment of inertia of the primary particle α, $\mathbf{F}_\alpha$ and $\mathbf{T}_\alpha$ are the force and torque acting on it, and $\mathbf{u}_\alpha$ and $\boldsymbol{\omega}_\alpha$ are its translational and angular velocity. For colloidal particles the inertial effects are generally negligible compared to the other involved forces and, consequently, Equations (16) can be reduced to the following form:

$$\begin{cases} \mathbf{F}_\alpha^H + \mathbf{F}_\alpha^{coll} \approx 0 \\ \mathbf{T}_\alpha^H + \mathbf{T}_\alpha^{coll} \approx 0 \end{cases} \tag{17}$$

Using Equation (7) from Stokesian dynamics for the hydrodynamic interactions, Equation (17) finally becomes:

$$[\mathcal{R}]\cdot\begin{Bmatrix} \mathbf{u}_1 - \mathbf{u}_\infty(\mathbf{x}_1) \\ \vdots \\ \mathbf{u}_N - \mathbf{u}_\infty(\mathbf{x}_N) \\ \boldsymbol{\omega}_1 - \boldsymbol{\omega}_\infty \\ \vdots \\ \boldsymbol{\omega}_N - \boldsymbol{\omega}_\infty \end{Bmatrix} = \begin{Bmatrix} \mathbf{F}_1^{coll} \\ \vdots \\ \mathbf{F}_N^{coll} \\ \mathbf{T}_{(1)}^{coll} \\ \vdots \\ \mathbf{T}_N^{coll} \end{Bmatrix} + [\mathcal{S}]\cdot\begin{Bmatrix} -\mathbf{E}_\infty \\ \vdots \\ -\mathbf{E}_\infty \\ -\mathbf{E}_\infty \\ \vdots \\ -\mathbf{E}_\infty \end{Bmatrix} \tag{18}$$

in which colloidal forces and torques are modelled by Equations (8), (10), (13), (14), (15). In this way the vectors $\mathbf{u}_\alpha - \mathbf{u}^\infty(\mathbf{x}_\alpha)$ and $\boldsymbol{\omega}_\alpha - \boldsymbol{\omega}^\infty$ are the only unknown variables. Hence, the solution of this set of equations gives the velocities of all the primary particles, from which particle trajectories can be obtained by an explicit Euler integration scheme.

The amplitude of the time step Δt is a critical parameter in the integration method. This is due to the steep variation of the forces with the distance between monomers, and care must be taken to properly simulate both lubrication effects and colloidal interaction. We adopted an adaptive scheme for the choice of the integration step: at every iteration we set the time step as $\Delta t = \min\left(\Delta t_b, \Delta t_{opt}\right)$, in which Δt_b is a base value chosen at the beginning of the simulation (in this case 10^{-7} s) and Δt_{opt} is the minimum among the optimal values estimated for all the monomer pairs (α,β) as:

$$\Delta t_{opt}^{\alpha,\beta} = \begin{cases} \frac{0.02z_0}{|\mathbf{u}_\alpha - \mathbf{u}_\beta|} & \text{if} \quad h < 10z_0 \\ \frac{0.5z_0}{|\mathbf{u}_\alpha - \mathbf{u}_\beta|} & \text{if} \quad h < 100z_0 \\ \frac{5z_0}{|\mathbf{u}_\alpha - \mathbf{u}_\beta|} & \text{otherwise} \end{cases} \tag{19}$$

where z_0 is the minimum approach distance of Equation (8). In this way we can reproduce accurately all the near-contact effects and safely adopt a longer time-step when monomers are far apart.

An encounter has to be simulated for a time long enough to allow the aggregates to approach from their initial positions, collide, and reach a stable configuration through the rearrangement

of the monomers. In non-dimensional terms, the time needed by the DEM simulation was estimated as:

$$\dot{\gamma} t_s = \frac{|z_j^0| - \left(R_i + R_j\right)}{y_j^0} + 4\pi n_{rot} \tag{20}$$

where the first term approximates the time required for contact (z_j^0 and y_j^0 are the initial coordinates of the aggregate j, while aggregate i is initially in the origin of the reference system); n_{rot} is the approximate number of rotations the newly generated aggregate undergoes before the DEM simulation is stopped, assuming an angular velocity of $\dot{\gamma}/2$. Even if this assumption may not be accurate for elongated aggregates,[58] test simulations showed that setting $n_{rot} = 8$ in Equation (20) gives a time large enough to ensure full relaxation of the newly generated aggregates, regardless of their overall morphology.

RESULTS AND DISCUSSION

We studied the process of shear aggregation for two different populations of primary particles: Population A composed by primary particles interacting only by means of central forces, and Population B in which primary particles are also subject to tangential forces upon contact. In both cases the samples simulated were very dilute (volume fraction of solid of 10^{-4} m^3/m^3) and initially composed by 200 spherical polystyrene particles with radius $a = 500$ nm. The particles were dispersed in water and exposed to a spatially uniform shear flow with a rate of 10 s^{-1}. Although the code is intrinsically capable of predicting the breakup of the aggregates, the simulations were stopped when the clusters were still relatively small, before any breakup event occurred. Indeed, according to the criterion by Vanni and Gastaldi for dilute systems,[34] the occurrence of breakup for our suspensions would require clusters more than 100 times bigger than the largest aggregates examined in the present work.

The values of the physical variables of the simulations are reported in Table 1. Neutrally buoyant solid particles were simulated. The elastic properties of the solid (elastic modulus and Poisson ratio) are typical of relatively compliant polymeric materials, such as polystyrene. Similarly, the value of Hamaker constant is typical of polymeric particles dispersed in a liquid medium.

Table 1. Physical properties of the simulated system

Parameter	Symbol	Value
Volume fraction of solid		10^{-4} m^3/m^3
Hamaker constant	A_H	$0.97 \cdot 10^{-20}$ J
Surface energy	γ_s	$4.7 \cdot 10^{-3}$ J$\cdot$m^{-2}
Minimum approach distance	z_0	0.165 nm
Monomer radius	a	500 nm
Medium viscosity	μ	10^{-3} Pa s
Medium density	ρ_l	1000 kg$\cdot$m^{-3}
Particle density	ρ_p	1000 kg$\cdot$m^{-3}
Shear rate	$\dot{\gamma}$	10 s^{-1}
Elastic modulus	E	3.4 GPa
Poisson ratio	ν	0.5
Tangential spring stiffness	k_t	$1.85 \cdot 10^{-5}$ N$\cdot$m^{-1}
Torsional spring stiffness	k_ϕ	$9.2 \cdot 10^{-18}$ N m rad^{-1}
Maximal spring elongation	ξ_{max}	50 nm
Maximal spring torsion	ϕ_{max}	0.10 rad

The set of parameters used herein leads to a Péclet number approximately equal to 6 for isolated monomers and to much larger values for clusters; in these conditions thermal motion has still a small role in monomer-monomer aggregation. However, for the sake of simplicity, we assumed encounter events to be driven uniquely by the gradient of the flow field, regardless of the actual size of the involved particles.

Dynamics of the Population and Size Evolution

The most direct consequence of aggregation is the increase of the mean particle size. In this regard Figure 5 shows the average number of primary particles per cluster $\langle P \rangle$ as a function of the dimensionless time $\dot{\gamma} t$ for the two populations. Ten encounter events elapsed between two subsequent points of the curves. The encounters which turned into aggregations determined the loss of aggregates from the population and increased the average size; on the contrary, the encounters which turned into missed aggregations left the population unaffected.

For both populations the rate of size growth (i.e. the slope of the curve) increased continuously throughout the aggregation process. This effect was already reported in the literature,[3,6] and is a consequence of the enhancement of the aggregation rate caused by the formation of larger aggregates with much bigger collision cross-section. The effect on the aggregation frequency, Equation (1), is proportional to the cube of the aggregate size and dominates over the reduction caused by the decrease of the concentration of suspended aggregates.

In the simulated time interval the number distribution of the aggregates is governed by the smallest clusters. As shown in Figure 6, monomers and dimers represent approximately 80 % of the populations and hence their effect predominates in the statistical variables based on the number distribution. Clearly, the geometry of monomers and dimers is fixed and is not influenced by the presence of tangential interactions. This is why the average size based on the number distribution $\langle P \rangle$ does not show relevant differences between the two populations.

Significant differences come out instead when looking at the evolution of statistical variables that are more sensitive to the biggest aggregates of the population, such as the average outer radius. Figure 7 illustrates the evolution of the Sauter diameter

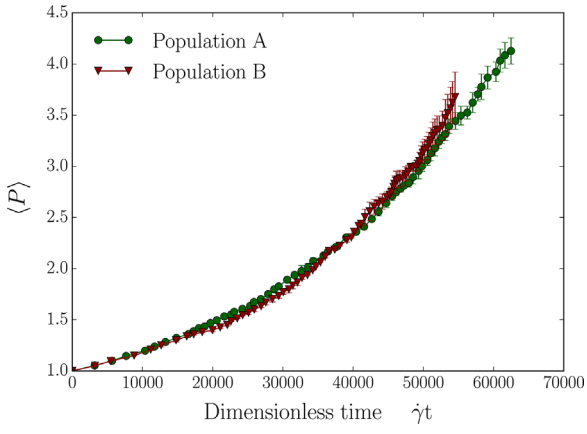

Figure 5. Time evolution of the average size of the suspended aggregates, expressed as the mean number of primary particles per cluster, for the two simulated populations. Each curve was obtained by averaging the data relative to three different realizations. The error bars indicate the standard deviation of the data.

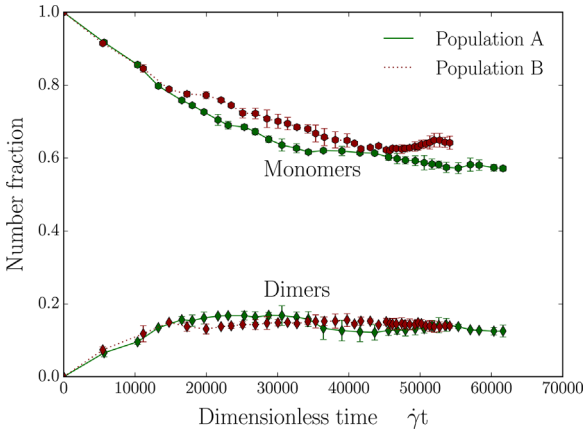

Figure 6. Time evolution of the number fractions of monomers and dimers.

d_{32} computed on the basis of the outer radius of the aggregates as:

$$d_{32} = 2 \cdot \frac{\sum_{i=1}^{N_a} R_i^3}{\sum_{i=1}^{N_a} R_i^2} \tag{21}$$

with N_a being the number of suspended aggregates; this average size characterizes the volume to surface ratio of the populations. Differently from $\langle P \rangle$, the Sauter diameters of the two populations coincide only in the initial part of the aggregation process. After about 25 000 time units, the curve relative to Population B exhibits a steep increase, reaching significantly larger values compared to Population A. This suggests that the aggregates of the two populations differ somehow in the characteristic morphology, although they are on average composed by the same number of primary particles.

From Figure 7 it is also apparent that Population A shows a monotonic and steady increase of d_{32}, whereas Population B exhibits also occasional reductions of this variable. These have not to be related to breakup events, but rather to the restructuring phenomena which involve clusters; even if an encounter did not turn into an aggregation, the DEM simulations frequently returned aggregates with slightly different morphology and more compact structure, because of the hydrodynamic interactions between

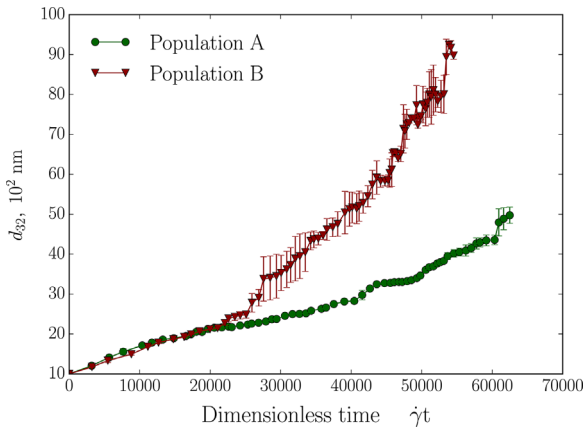

Figure 7. Evolution of the average size of the suspended aggregates in terms of Sauter diameter, Equation (21). The error bars show the standard deviation of the data as estimated from three different realizations.

approaching aggregates. This feature is not present in Population A, in which compaction phenomena are much faster and take place soon after a new aggregate is generated. Population B also shows a noticeably larger scatter of data among the different realizations, meaning that a wider variety of structures are produced upon aggregation.

Aggregate Characterization

The clusters of the two populations of aggregates are significantly different in their morphological properties. In order to give an overview of these different features, Figure 8 reports the geometry of a small sample of the populations of clusters. Each line of the figure compares two clusters with a similar number of primary particles P. It is immediately apparent that the clusters from Population A are more compact than those from Population B. They also show smaller outer radius R and a larger number of contacts per primary particle $\langle n_c \rangle$. Conversely, the aggregates of Population B have a more elongated shape with larger aspect ratio (A.R.) and frequently exhibit branches extending from a central core. Below, these considerations will be elaborated in a more quantitative way, by characterizing statistically the structure of the formed aggregates at both a local and global level.

Local structure: coordination number and trimer angle

A relevant piece of information on the structure of colloidal aggregates is given by the number of monomer-monomer bonds, as this number provides a measure of the compactness of the cluster structure. Figure 9 illustrates the relationship between the number of primary particles P composing the clusters of the population and the average coordination number $\langle n_c \rangle = 2n_b/P$, with n_b being the number of bonds detected in the aggregate.

For both populations the average coordination number $\langle n_c \rangle$ increases with the size of the cluster: obviously, in small clusters most of the particles are located in the outer region of the aggregate, exposed to the dispersing medium and thus involved in a small number of contacts; on the contrary, in large clusters, the fraction of primary particles in the internal region of the structure is much bigger. Such particles are responsible for the increase of $\langle n_c \rangle$ because they are involved in a larger number of bonds, being fully surrounded by other primary particles.

Apart from this similarity, a striking difference in the values of $\langle n_c \rangle$ for the two populations stands out. The primary particles of Population A, interacting only via central interactions, form aggregates characterized by closely packed structures with average coordination numbers close to 6 for the biggest clusters; in these aggregates the primary particles are free to slide and roll over each other, thereby making clusters to soon reach a compact structure under the effect of the viscous shear stresses. On the contrary, the presence of tangential interactions in Population B prevents the generation of a compact arrangement and indeed the clusters of this population are highly porous. From a structural point of view, the smallest aggregates of Population B can be classified as isostatic and their coordination number equals $2(P-1)/P$, according to the criterion by Gastaldi and Vanni.[59] Isostatic aggregates are obtained when each aggregation event proceeds through the generation of a single new interparticle bond between the two parent aggregates, with the structure of the newly generated aggregate being frozen after generation. With Population B such a situation occurs when the aggregates are relatively small, while bigger aggregates present an average coordination number slightly larger than the isostatic one because of internal restructuring. The restoring forces arising from tangential interactions are not always able

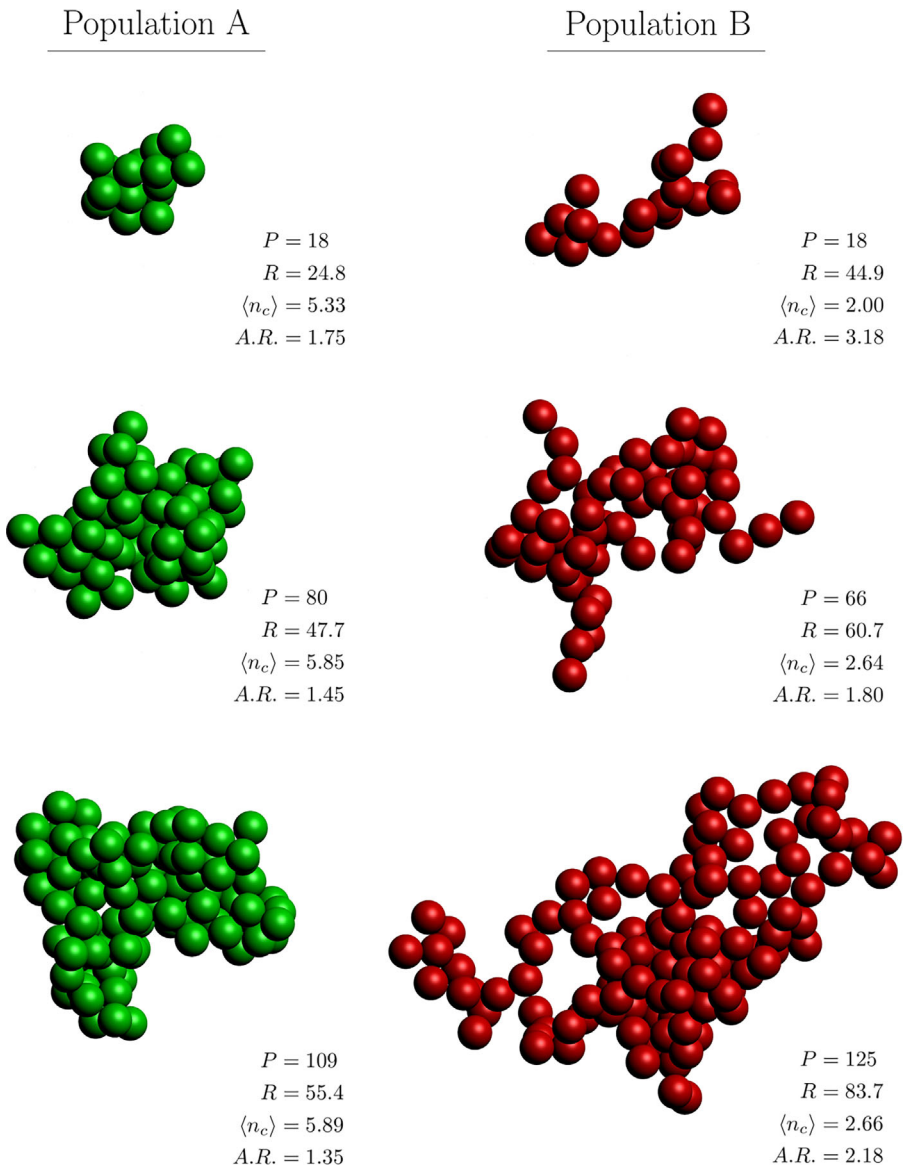

Figure 8. A small sample of the two populations of clusters.

to indefinitely hinder the relative motion of adjacent particles along the contact surface; in these aggregates the stresses generated by the dispersing medium are propagated and accumulated along the filaments of the structure, causing the bond tangential or bending resistance to be exceeded in some locations, if the filament is long enough. As a consequence, restructuring phenomena may take place, increasing the number of contacts and making large clusters slightly over-constrained.

Another indicator of the cluster local structure is the mean three particle angle $\langle\theta\rangle$, plotted as a function of P in Figure 10. To compute $\langle\theta\rangle$ all the existing groups of three connected primary particles in the cluster were identified and characterized by the trimer angle $\theta_{\alpha\gamma\beta}$, formed by the two straight lines passing through the centre of the intermediate particle γ and through the centres of the other two particles α and β; the angle $\theta_{\alpha\gamma\beta}$ was computed as:

$$\theta_{\alpha\gamma\beta} = 2 \cdot \arcsin\left(\frac{d_{\alpha\beta}}{4a}\right) \tag{22}$$

where $d_{\alpha\beta}$ is the centre-to-centre distance between particles α and β. For rigid particles the angle can vary from 60°, corresponding to particles that form an equilateral triangle, to 180°, corresponding to particles aligned in a straight chain. However, it is worth mentioning that angles slightly smaller than 60° were also observed, because of the deformation of the contact region predicted by the JKR theory.

Both classes of clusters reach an asymptotic value of $\langle\theta\rangle$ as the number of constituent primary particles increases; this asymptote is approximately equal to 87° for the aggregates of Population A and to 105° for those of Population B, confirming that the primary particles are assembled in a quite different manner in the two populations. The larger angles of Population B show that these clusters have a more open and tenuous structure compared to those of Population A. The asymptotic angle of Population B is very close to the value reported for synthetic DLCA clusters.[60] This fact indicates that the morphology of rigid aggregates is influenced mainly by the condition of destabilization (full or partial), whereas the type of aggregation (perikinetic or orthokinetic) plays

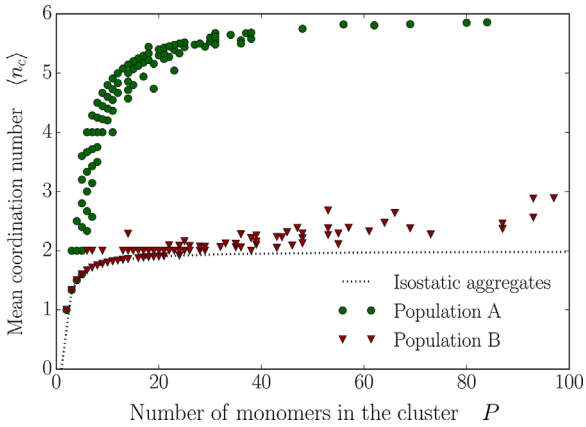

Figure 9. Mean coordination number for the two populations of clusters.

a minor role. Indeed, the fractal dimension also has similar values (around 1.8) in both perikinetic and orthokinetic aggregation for fully destabilized suspensions.

It is also apparent that a wider scatter of the data characterizes Population B, especially for small cluster size, indicating that a greater variety of shapes exists. On the contrary, the smaller clusters of Population A present a more recurrent pattern, due to the fact that upon contact a large-scale restructuring occurs, always ending in a compact structure.

Global scale structure: aspect ratio

The response of a complex aggregate to the fluid flow is very similar to the response of an ellipsoid with the same inertia matrix as the aggregate.[61] Due to this reason, the geometric properties of an aggregate are often expressed in terms of those of the inertia-equivalent ellipsoid. In particular, we define the aspect ratio of a cluster as:

$$A.R. = \frac{2a_1}{a_2 + a_3} \tag{23}$$

where a_1 is the major semi-axis of the equivalent ellipsoid and a_2, a_3 are the two minor ones. Equation (23) returns values close to 1 for round-shaped aggregates and substantially larger values for rod-shaped ones.

In order to calculate the lengths of the semi-axes, we start from the inertia tensor of a single primary particle α with respect to its centre of mass, $\mathbf{I}_\alpha = (2/5) m_\alpha a^2 \mathbf{i}$, where $\mathbf{i}$ is the identity tensor and m_α the mass of the primary particle. Subsequently, in order to obtain the inertia tensor relative to the centre of mass of the aggregate, we applied the parallel axis theorem in its tensorial formulation to the inertia tensor of each primary particle α as:

$$\mathbf{I}'_\alpha = \mathbf{I}_\alpha + m_\alpha \left(\left| (\mathbf{x}_\alpha - \mathbf{x}_{cm}) \right|^2 \mathbf{i} - (\mathbf{x}_\alpha - \mathbf{x}_{cm})(\mathbf{x}_\alpha - \mathbf{x}_{cm}) \right) \tag{24}$$

where $\mathbf{x}_\alpha$ is the position vector of the α monomer and $\mathbf{x}_{cm}$ identifies the position of the centre of mass of the aggregate. Finally, the inertia tensor of the whole cluster was obtained as:

$$\mathbf{I}_{cluster} = \sum_\alpha \mathbf{I}'_\alpha \tag{25}$$

The principal moments of inertia ($I_1 > I_2 > I_3$) of the cluster were computed by diagonalization of $\mathbf{I}_{cluster}$ and the length of the principal semi-axes ($a_1 > a_2 > a_3$) are given by the following equations:[62]

$$\begin{aligned} a_1 &= \sqrt{\frac{5}{2} \frac{I_2 + I_3 - I_1}{\sum_\alpha m_\alpha}} \\ a_2 &= \sqrt{\frac{5}{2} \frac{I_1 + I_3 - I_2}{\sum_\alpha m_\alpha}} \\ a_3 &= \sqrt{\frac{5}{2} \frac{I_1 + I_2 - I_3}{\sum_\alpha m_\alpha}} \end{aligned} \tag{26}$$

Figure 11 shows the distribution of the aspect ratio for the two populations of aggregates sampled after 600 encounters from the beginning of the aggregation process.

The distribution of aspect ratio for the clusters of Population A exhibits a peak at low values (around 1.5), meaning that most of the clusters have a spheroidal shape. High values of aspect ratio (i.e. larger than 2.5) are obtained only by the biggest aggregates, which are quite few in comparison to the small ones. Differently, the aggregates of Population B have a broader variety of structures; a peak of the distribution is detectable for $A.R. \approx 2$, but its height is significantly lower than the peak of Population A. Moreover a long tail extending up to values of

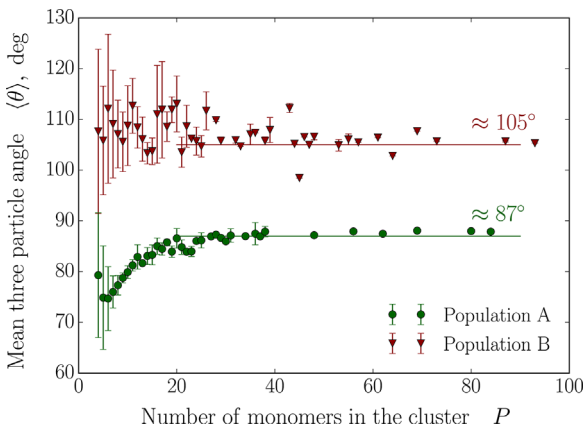

Figure 10. Average three particle angle as a function of the number of constituent primary particles.

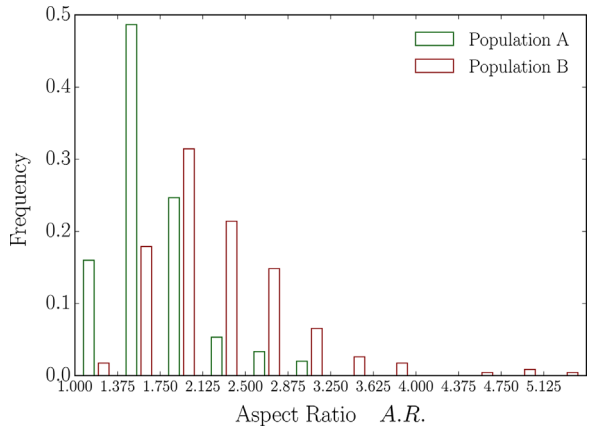

Figure 11. Distribution of the aspect ratio for the two populations. Only clusters composed by at least 5 primary particles are considered.

aspect ratio larger than 5 characterizes this distribution. For this population only minor rearrangement may take place and the open and elongated structure generated at the very first contact is preserved during the aggregation process, whereas the ability of the monomers of Population A to mutually slide and roll at contact generates compact structures, which are less elongated.

The aspect ratio has a strong impact on the collision rate and has to be accounted for in order to explain the similar rate of aggregation of the examined classes of particles. Indeed, at first sight one would expect faster aggregation for Population B, because of the larger radius of these aggregates (Figure 7), which gives a much larger encounter cross-section with respect to the compact aggregates of Population A. On the contrary, the aggregation rate is nearly the same for both populations, as is apparent from the evolution of the mean aggregate size $\langle P \rangle$ reported in Figure 5. As shown by the aspect ratio, the aggregates of Population B are highly elongated and thus, while rotating in the shear flow, they spend most of their time aligned or partially aligned with the fluid flow,[34,62] making the contact more difficult during an encounter and reducing significantly the collision efficiency. Hence, the joint effect of the larger encounter cross-section and reduced collision efficiency for clusters B makes their aggregation rate similar to that of aggregates A.

Mass-size scaling law

Aggregates are often characterized on the basis of their gyration radius R_g, which is defined as the root-mean-square distance of the monomers from the centre of mass of the aggregate and, for a cluster composed by P primary particles, reads as:

$$R_g = \sqrt{\frac{1}{P}\sum_{\alpha}^{P} |\mathbf{x}_\alpha - \mathbf{x}_{cm}|^2} \tag{27}$$

We attempted to relate the gyration radius of the two populations of aggregates to the number of constituent primary particles by means of a power law of the following kind:

$$P = k_f \cdot \left(R_g/a\right)^{d_f} \tag{28}$$

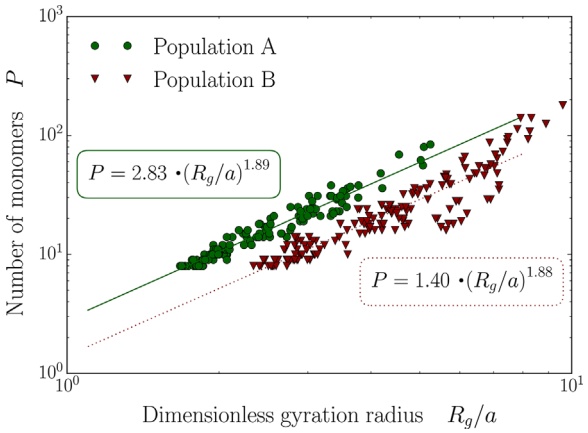

Figure 12. Number of monomers P versus dimensionless gyration radius R_g/a for the two populations of aggregates in a log-log plot. In the rectangles the power-law equations of the fitting lines are reported.

where the two parameters are the pre-factor k_f and the power-law exponent d_f. Both parameters were determined by fitting the set of data $(P, R_g/a)$ relative to the populations of particles with Equation (28). The aggregates employed for the estimation of d_f and k_f were drawn by sampling the populations every 100 encounter events and excluding the clusters composed by less than 8 primary particles. The results are shown in Figure 12. As is apparent, the two populations exhibit very similar values of the power-law exponent, whereas a quite large difference exists between their pre-factors, with that relative to Population A being twice as large as that of Population B.

As is well known, rigid aggregates have a fractal structure and the power-law exponent is their fractal dimension.[63,64] Values of d_f around 1.80 and pre-factors around unity are typical of rigid aggregates produced in fully destabilized colloidal suspensions, in which all collisions between clusters lead to a permanent and rigid bond. These conditions are close to those adopted for the generation of population B. The slightly higher values for the exponent (1.88) and pre-factor (1.40) are likely due to the presence of a level of restructuring after contact, which is witnessed by the coordination number, as discussed previously.

In spite of the similar value of power law exponent, the aggregates of Population A have very different features. They are compact and do not exhibit the sequence of dense and void region that is typical of fractal objects with small fractal dimension. On the contrary, all the primary particles are confined in a narrow region of space, where the solid density is close to that of random close packed structures. These aggregates are not rigid and undergo different deformations in the flow field, depending on their size. The smallest clusters normally retain a spheroidal shape, while the largest aggregates can be stretched more easily and become partially elongated in the shear flow. Indeed, it is this gradual change of shape with size that is reflected by the small value (1.89) of the power law exponent for this population and not the presence of a fractal structure.

In the plot a significant deviation of the data from the fitting lines is noticeable for both populations, although it is more intense for Population B. As pointed out by Heinson et al.,[65,66] this behaviour may be a consequence of the broad variety of shapes and aspect ratios exhibited by these clusters. This fact suggests that a complex interplay between the aspect ratio, the power-law exponent, and the pre-factor may exist and therefore all these parameters appear as essential ingredients for a full characterization of a population of clusters.

CONCLUSIONS

In the present work we introduced a mixed deterministic-stochastic method able to simulate the process of shear-induced aggregation in destabilized colloidal suspensions. The method is built on the combination of a Monte Carlo algorithm, used to sample a statistically expected sequence of encounter events between suspended aggregates, with a Discrete Element Method (DEM), built in the framework of Stokesian dynamics, able to simulate in a fully deterministic manner the outcome of each encounter event. This combination allowed us to simulate dynamically the aggregation process of populations of colloidal clusters.

Simulations were carried out starting from monodisperse polystyrene primary particles. The aggregation behaviour of two different populations of particles was simulated: the first

population was composed by primary particles interacting only by means of central forces, arising from Van der Waals interactions and JKR contact forces; in the second population primary particles were capable of withstanding also mutual sliding and rolling by the onset of tangential interaction upon contact; to model such interactions we implemented a spring-like model recently built on the basis of experimental evidence.

Results showed that substantial differences in the cluster morphology appear when introducing tangential interactions at contact: when counting for such interactions, primary particles aggregate forming rigid structures that are porous and branched, and characterized by low values of the coordination number. The absence of tangential interaction, instead, causes primary particles to be free to slide and roll over each other, leading to the formation of dense and highly connected clusters. This difference has also an impact on the global shape of the clusters: a more regular and less elongated shape was observed for clusters produced upon aggregation of particles interacting only by central forces. This is a consequence of the intense restructuring phenomena these clusters are subject to under the viscous shear stress. Conversely, a greater variety of shapes and aspect ratios characterizes the cluster formed by primary particles interacting both centrally and tangentially; for these clusters restructuring phenomena are hindered as long as the viscous stresses do not exceed the single bond tangential resistance.

The mass-size power law gives similar values of the power-law exponent for the two populations of clusters. Such a value, however, reflects two very different features of the populations: a true low-density fractal structure in the presence of tangential interaction, and a size-dependent shape of the clusters when tangential interaction is absent.

NOMENCLATURE

a	primary particle radius (m)
a_1,a_2,a_3	principal semi-axes length (m)
A_H	Hamaker constant (J)
$A.R.$	cluster aspect ratio
b_0	zero-load contact radius (m)
c	aggregate number concentration (m^{-3})
d_f	power-law exponent
d_{32}	Sauter diameter (m)
$\mathbf{e}$	unit vector
E	elastic modulus (Pa)
$\mathbf{E}$	strain rate tensor (s^{-1})
f	encounter frequency (s^{-1})
$\mathbf{F}$	force (N)
h	surface-to-surface distance (m)
$\mathbf{i}$	identity tensor
$\mathbf{I}$	inertia tensor ($kg{\cdot}m^2$)
k_f	power-law prefactor
k_t	tangential spring stiffness ($N{\cdot}m^{-1}$)
k_ϕ	torsional spring stiffness ($N{\cdot}m{\cdot}rad^{-1}$)
N	number of primary particles in the DEM simulation
N_a	number of aggregates
n_c	coordination number
P	number of primary particle in a cluster
Pr	probability
R	aggregate outer radius (m)
R_g	gyration radius (m)
$\mathbf{T}$	torque (N·m)
t	time (s)
$\mathbf{u}$	velocity ($m{\cdot}s^{-1}$)
$\mathbf{x}$	position vector (m)
x, y, z	components of $\mathbf{x}$ (m)
z_0	minimum approach distance (m)

Greek Letters

$\dot{\gamma}$	shear rate intensity (s^{-1})
γ_s	superficial energy ($N{\cdot}m^{-1}$)
δ	lubrication cut-off length (m)
ΔV	simulated volume (m^3)
ε	corrective factor for the encounter cross-section
θ	three-particle angle (rad)
λ	London wavelength (m)
μ	liquid viscosity (Pa·s)
ν	Poisson ratio
$\boldsymbol{\xi}$	spring elongation vector
ξ_{max}	maximal spring elongation (m)
ρ	density ($kg{\cdot}m^{-3}$)
ϕ	torsional spring angle (rad)
ϕ_{max}	maximal spring torsion (rad)
$\boldsymbol{\omega}$	angular velocity ($rad{\cdot}s^{-1}$)

Subscripts

cm	aggregate centre of mass
i,j	aggregate indexes
l	liquid
p	particle
α,β,γ	primary particle indexes
∞	undisturbed flow field

Superscripts

$coll$	colloidal
H	hydrodynamic

REFERENCES

[1] V. Oles, *J. Colloid Interf. Sci.* **1992**, *154*, 351.

[2] T. Serra, J. Colomer, X. Casamitjana, *J. Colloid Interf. Sci.* **1997**, *187*, 466.

[3] K. A. Kusters, J. G. Wijers, D. Thoenes, *Chem. Eng. Sci.* **1997**, *52*, 107.

[4] J. C. Flesch, P. T. Spicer, S. E. Pratsinis, *AIChE J.* **1999**, *45*, 1114.

[5] V. A. Tolpekin, M. H. G. Duits, D. Van Den Ende, J. Mellema, *Langmuir* **2004**, *20*, 2614.

[6] L. Wang, D. L. Marchisio, R. D. Vigil, R. O. Fox, *J. Colloid Interf. Sci.* **2005**, *282*, 380.

[7] D. Marchisio, M. Soos, J. Sefcik, M. Morbidelli, *AIChE J.* **2006**, *52*, 158.

[8] D. Ramkrishna, *Population balances: Theory and applications to particulate systems in engineering*, 1st edition, Academic Press, San Diego **2000**.

[9] D. L. Marchisio, R. O. Fox, *Computational models for polydisperse particulate and multiphase systems*, 1st edition, Cambridge University Press, Cambridge **2013**.

[10] M. V. Smoluchowski, *Z. Phys. Chem.* **1917**, *92*, 129.

[11] M. Kostoglou, A. J. Karabelas, *J. Colloid Interf. Sci.* **1994**, *163*, 420.

[12] M. Vanni, *J. Colloid Interf. Sci.* **2000**, *221*, 243.

[13] M. Kostoglou, A. G. Konstandopoulos, S. K. Friedlander, *J. Aerosol Sci.* **2006**, *37*, 1102.

[14] J. Kumar, M. Peglow, G. Warnecke, S. Heinrich, *Comput. Chem. Eng.* **2008**, *32*, 1810.
[15] R. McGraw, *Aerosol Sci. Tech.* **1997**, *27*, 255.
[16] D. L. Marchisio, R. D. Vigil, R. O. Fox, *J. Colloid Interf. Sci.* **2003**, *258*, 322.
[17] A. Buffo, M. Vanni, D. L. Marchisio, R. O. Fox, *Int. J. Multiphas. Flow* **2013**, *50*, 41.
[18] K. Liffman, *J. Comput. Phys.* **1992**, *100*, 116.
[19] M. Smith, T. Matsoukas, *Chem. Eng. Sci.* **1998**, *53*, 1777.
[20] F. E. Kruis, A. Maisels, H. Fissan, *AIChE J.* **2000**, *46*, 1735.
[21] A. Zucca, D. L. Marchisio, M. Vanni, A. A. Barresi, *AIChE J.* **2007**, 53, 918.
[22] H. Zhao, C. Zheng, *J. Comput. Phys.* **2009**, *228*, 1412.
[23] P. A. Cundall, O. D. L. Strack, *Geotechnique* **1979**, *29*, 47.
[24] L. Isella, Y. Drossinos, *Phys. Rev. E* **2010**, *82*, 011404.
[25] V. Becker, E. Schlauch, M. Behr, H. Briesen, *J. Colloid Interf. Sci.* **2009**, *339*, 362.
[26] V. Becker, H. Briesen, *J. Colloid Interf. Sci.* **2010**, *346*, 32.
[27] M. L. Eggersdorfer, D. Kadau, H. J. Herrmann, S. E. Pratsinis, *J. Colloid Interf. Sci.* **2010**, *342*, 261.
[28] M. Kroupa, M. Vonka, J. Kosek, *Langmuir* **2014**, *30*, 2693.
[29] M. Kroupa, M. Vonka, M. Soos, J. Kosek, *Langmuir* **2015**, *31*, 7727.
[30] K. Higashitani, K. Iimura, *J. Colloid Interf. Sci.* **1998**, *204*, 320.
[31] K. Higashitani, K. Iimura, H. Sanda, *Chem. Eng. Sci.* **2001**, *56*, 2927.
[32] S. Harada, R. Tanaka, H. Nogami, M. Sawada, *J. Colloid Interf. Sci.* **2006**, *301*, 123.
[33] R. Seto, R. Botet, H. Briesen, *Phys. Rev. E* **2011**, *84*, 041405.
[34] M. Vanni, A. Gastaldi, *Langmuir* **2011**, *27*, 12822.
[35] Y. M. Harshe, M. Lattuada, *Langmuir* **2011**, *28*, 283.
[36] Y. M. Harshe, M. Lattuada, M. Soos, *Langmuir* **2011**, *27*, 5739.
[37] Y. M. Harshe, M. Lattuada, *Langmuir* **2012**, *28*, 283.
[38] R. Seto, R. Botet, G. Auernhammer, H. Briesen, *Eur. Phys. J. E* **2012**, *35*, 1.
[39] J. De Bona, A. S. Lanotte, M. Vanni, *J. Fluid Mech.* **2014**, *755*, 365.
[40] K. Horii, R. Yamada, S. Harada, *Langmuir* **2015**, *31*, 7909.
[41] M. Vanni, *Comput. Phys. Commun.* **2015**, *192*, 70.
[42] Y. M. Harshe, M. Lattuada, *J. Phys. Chem. B* **2016**, *120*, 7244.
[43] J. P. Pantina, E. M. Furst, *Phys. Rev. Lett.* **2005**, *94*, 138301.
[44] J. P. Pantina, E. M. Furst, *Langmuir* **2008**, *24*, 1141.
[45] V. Becker, H. Briesen, *Phys. Rev. E* **2008**, *78*, 061404.
[46] J. S. Marshall, *J. Comput. Phys.* **2009**, *228*, 1541.
[47] G. Inci, A. Arnold, A. Kronenburg, R. Weeber, *Aerosol Sci. Tech.* **2014**, *48*, 842.
[48] B. H. Shah, D. Ramkrishna, J. D. Borwanker, *AIChE J.* **1977**, *23*, 897.
[49] J. F. Brady, G. Bossis, *Annu. Rev. Fluid Mech.* **1988**, *20*, 111.
[50] L. Durlofsky, J. F. Brady, G. Bossis, *J. Fluid Mech.* **1987**, *180*, 21.
[51] S. Kim, K. J. Karrila, *Microhydrodynamics: Principles and Selected Applications*, 2nd edition, Dover Publications, Mineola **2005**.
[52] M. Trulsson, B. Andreotti, P. Claudin, *Phys. Rev. Lett.* **2012**, *109*, 118305.
[53] R. Seto, R. Mari, J. F. Morris, M. M. Denn, *Phys. Rev. Lett.* **2013**, *111*, 218301.
[54] R. Mari, R. Seto, J. F. Morris, M. M. Denn, *J. Rheol.* **2014**, *58*, 1693.
[55] H. C. Hamaker, *Physica* **1937**, *4*, 1058.
[56] M. Vanni, G. Baldi, *Adv. Colloid Interfac.* **2002**, *97*, 151.
[57] K. L. Johnson, K. Kendall, A. D. Roberts, *P. Roy. Soc. A-Math. Phy.* **1971**, *324*, 301.
[58] G. Frappier, B. S. Lartiges, S. Skali-Lami, *Langmuir* **2010**, *26*, 10475.
[59] A. Gastaldi, M. Vanni, *J. Colloid Interf. Sci.* **2011**, *357*, 18.
[60] A. D. Melas, L. Isella, A. G. Kostandopoulos, Y. Drossinos, *J. Colloid Interf. Sci.* **2014**, *417*, 27.
[61] Y. M. Harshe, L. Ehrl, M. Lattuada, *J. Colloid Interf. Sci.* **2010**, *352*, 87.
[62] L. Sanchez Fellay, C. Twist, M. Vanni, *Acta Mech.* **2013**, *224*, 2225.
[63] R. Jullien, R. Botet, *Aggregation and Fractal Aggregates*, 1st edition, World Scientific, Singapore **1987**.
[64] P. J. Meakin, *J. Sol-Gel Sci. Techn.* **1999**, *14*, 97.
[65] W. R. Heinson, C. M. Sorensen, A. Chakrabarti, *Aerosol Sci. Tech.* **2010**, *44*, i.
[66] W. R. Heinson, C. M. Sorensen, A. Chakrabarti, *J. Colloid Interf. Sci.* **2012**, *375*, 65.

Manuscript received November 13, 2016; revised manuscript received February 3, 2017; accepted for publication March 10, 2017